

Sulfur and sulfur-oxide compounds as potential optically active defects on SWCNTs

Tina N. Mihm,¹ K. Jing Trerayapiwat,² Xinxin Li,^{2,3} Xuedan Ma,^{2,4,5} and Sahar Sharifzadeh^{1,6,7,8, a)}

¹⁾ *Department of Electrical and Computer Engineering, Boston University, MA, 02215, USA*

²⁾ *Center for Nanoscale Materials, Argonne National Laboratory, Lemont, IL 60439, USA*

³⁾ *Consortium for Advanced Science and Engineering, University of Chicago, Chicago, IL 60637, USA*

⁴⁾ *Materials Science and NanoEngineering, Rice University, Houston, TX, 77251, USA*

⁵⁾ *Northwestern Argonne Institute of Science and Engineering, Evanston, IL 60208, USA*

⁶⁾ *Department of Chemistry, Boston University, Boston, MA, 02215, USA*

⁷⁾ *Materials Science Division, Boston University, Boston, MA, 02215, USA*

⁸⁾ *Department of Physics, Boston University, Boston, MA, 02215, USA*

(Dated: September 30, 2024)

Semiconducting single-walled carbon nanotubes (SWCNT) containing sp^3 -type defects are a promising class of optoelectronic materials, demonstrating single photon emission and long-lived spins. The defect introduces new optical transitions due to both symmetry breaking induced band splitting and introduction of in-gap electronic states. We investigate sulfur-oxide containing compounds as a new class of optically active dopants on (6,5) SWCNT. The SWCNT is exposed to sodium dodecyl sulfate with the resulting compound displaying a red-shifted and bright photoluminescence peak that is characteristic of sp^3 doping. Density functional theory calculations are then performed on the adsorbed compounds that may arise (S, SO, SO₂ and SO₃). These calculations indicate that the two smallest molecules strongly bind to the SWCNT with binding energies of $\sim 1.5 - 1.7$ eV and 0.56 eV for S and SO, respectively. Moreover, these adsorbates introduce in-gap electronic states into the bandstructure of the tube consistent with the measured red-shift of (0.1 – 0.3) eV. Our study suggests that sulfur-based compounds are promising new dopants for (6,5) SWCNT with tunable electronic properties.

Doped semiconducting single walled carbon nanotubes (SWCNT) show promise as optical sensors¹ and quantum light emitters² due to their controlled sensitivity to adsorbates and tunable electron fluorescence.^{1,3-5} For this class of materials, covalent defects introduce new optical transitions that modify the optical absorption spectrum and increase the photoluminescence (PL) efficiency.⁴⁻¹¹ As such, defective SWCNT display high purity single photon emission (SPE) with improved quantum yields^{3,4,8,9,11} for incorporation into bioelectronic devices,^{12,13} sensors¹ and quantum devices.^{2,14}

Dopants are typically introduced to the SWCNT through breaking of one carbon sp^2 bond and attaching a ligand that creates an sp^3 defect site. This defect can create a deep trap state (~ 100 meV) that localizes the exciton and significantly improves SPE.^{2,3,7,10,15-17} The most common sp^3 defects are atomic defects, such as hydrogen¹⁸ and oxygen,^{4,7,9,16} and functionalized aryl groups.^{8,10,17,19,20} The atomic defects, particularly oxygen, form at stable locations on the tube, with a red-shift of the photoluminescence (PL) peak and enhanced photon emissions.^{4,7,9} However, the resulting electronic properties of atomic defects synthesized thus far are determined only by the defect binding configuration, limiting

the ability to modify their electronic properties.¹⁶ On the other hand, aryl groups and carbon chain dopants offer stable defect sites with slightly more tunability through their functional groups.^{2,8,10,17,19} However, the electronic structure of these molecular-based dopants is hard to control when passivated,^{5,21-23} and has been shown to be defect-independent in certain unpassivated aryl groups.²⁴ Given the close similarities between the limitations of atomic and aryl sp^3 -defects, we explore atomic-like defects, which may provide a practical path for creating doped SWCNT for lower cost of materials that can be produced on an industrial scale.

In this Letter, we present an investigation of new sulfur-oxide-based dopants for (6,5) SWCNT. Similar to oxygen, sulfur oxides are easy to obtain as reactants and so we investigate whether these defects can produce optically active states similar to prior sp^3 defects. By introduction of sodium dodecyl sulfate to solution-phase (6,5) SWCNT, which we expect results in SO₂ adsorption on the surface, we show that a new doped species is created with the desired red-shifted emissions spectrum as shown in Figure 1. Within density functional theory (DFT), we study the adsorption of sulfur-oxide derivatives that may arise (S, SO, SO₂, SO₃) in order to determine the most likely species that has been synthesized. We predict that the larger two molecules studied, SO₂ and SO₃, are weakly physisorbed to the SWCNT, with little to

^{a)} Electronic mail: ssharifz@bu.edu

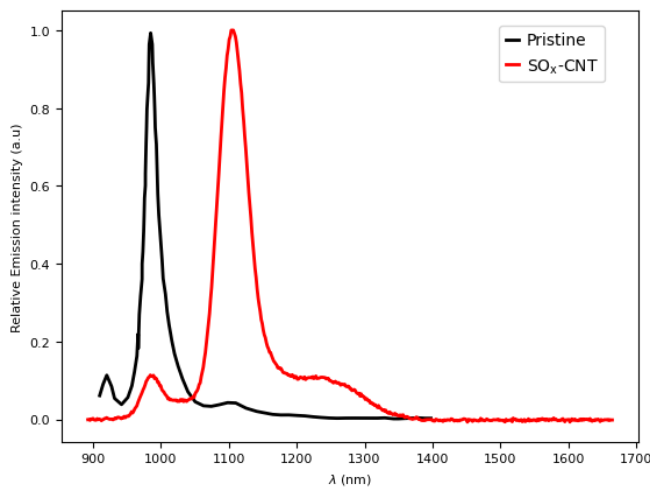


Figure 1. Photoluminescence spectrum of pristine (6,5) SWCNT and (6,5) SWCNT after exposure to sodium dodecyl sulfate. The data for each plot was normalized such that the maximum intensity is 1 (see SI Fig S.1 for measured spectrum of the doped SWCNT). The pristine spectrum was extracted from Ref 7.

no electronic interaction to the tube. In contrast, S and SO favorably bind to the tube with a red-shifted gap due to either defect-induced band splitting or introduction of an in-gap defect state. Thus, our study indicates that S and SO defects can be incorporated into and tune the optical properties of (6,5) SWCNT.

Figure 1 presents the photoluminescence (PL) spectrum for the SO_x -doped (6,5) SWCNT compared with the pristine tube. The peak maximum is at 1105 nm (1.12 eV) with a low-energy shoulder at 1228 nm (1.0 eV) and another peak at 984 nm (1.26 eV) that is consistent with the pristine tube E_{11} peak⁷. The fact that new transitions are introduced at 0.1 – 0.3 eV below the pristine gap is consistent with sp^3 doping of the (6,5) SWCNT.^{7,16,19,25} The details of synthesis and characterization of this system will be published elsewhere. Here, we focus on better understanding the chemical nature and electronic structure of this new species from first-principles DFT simulations.

Figure 2(a) shows the different sulfur compounds considered along with their corresponding binding configuration relative to the SWCNT. We chose S, SO, SO_2 , and SO_3 because of prior spectroscopic studies combined with electron microscopy that determined SO_2 may decompose into these compounds on SWCNT.²⁶ We considered different possible configurations of the adsorbate and only show configurations with favorable binding here (see supporting information Section 2.1 for details on unbound structures). For the single sulfur atom, we considered epoxide-type and ether-type binding (structures 1 and 2), both of which have been shown to be energetically favorable locations for oxygen binding on (6,5) SWCNT.¹⁶ For the SO molecule, a four-member ring-type binding (structure 3) with the S and O each bound to one carbon atom was found to be favorable. For each S and SO configuration, we consider two different orien-

Table I. Adsorption energy (E_b), band gap (E_{gap}), and the energies of the highest valence band (E_{VBM}) and lowest unoccupied state (E_{LUS}) for the defects considered in this work. The adsorption energies are defined such that a negative energy is bound (see Eq. (1)). All energies are in eV.

Structure	E_b	E_{VBM}	E_{LUS}	E_{gap}
S, Episulfide-l	-1.53	-3.55	-2.91	0.64
S, Thioether-l	-1.53	-3.55	-2.91	0.64
S, Thioether-d	-1.69	-3.60	-2.72	0.88
SO, 1,2-oxathietane-l	-0.56	-3.62	-2.78	0.84
SO, 1,2-oxathietane-d	-0.56	-3.62	-2.78	0.84
SO_2 , OO-loop-d	-0.20	-3.64	-2.73	0.92
SO_2 , Episulfide-d	-0.20	-3.64	-2.73	0.91
SO_2 , Line-H ^a	-0.33	-3.39	-2.73	0.66
SO_3 , flat	-0.27	-3.63	-2.75	0.88
Pristine	–	-3.62	-2.70	0.92

^a The binding energy for SO_2 was calculated by subtracting off the hydrogen binding energy from the total binding energy. See computational details.

tations of the C-S-C bonds, along the long (‘l’) and short (‘d’) axes of the tube (see Fig. 2(b)). For SO_2 , three different binding configurations were found to be favorable: 1) the SO_2 attached to two carbons across a broken carbon bond via the two oxygen on the SO_2 labeled “OO-loop” (structure 4), inspired by the orientation of SO_2 bound to graphene sheets;^{27,28} 2) the episulfide-type binding, a modification of the epoxide-type binding of S (structure 5); and 3) with a hydrogen atom attached to a carbon atom neighboring the adsorption site, with the O’s on the SO_2 oriented to be in line with the hydrogen, labeled “Line-H” (structure 6), introduced to test whether H can increase the affinity of the adsorbate to the tube. Lastly, for SO_3 , a flat-type binding motivated by binding of SO_3 on graphene is found to be favorable (structure 7).²⁹

We present the binding energies of the sulfur compounds to (6,5) SWCNT in Table I, calculated as,

$$E_b = E_{\text{CNT}+\text{SO}_x} - (E_{\text{CNT}} + E_{\text{SO}_x}). \quad (1)$$

Here, the $E_{\text{CNT}+\text{SO}_x}$ is the total energy of the adsorbate on SWCNT, E_{CNT} is the total energy of the pristine tube, and E_{SO_x} is the total energy of the sulfur compound in vacuum.

The S atom is the most strongly bound to the tube, with binding energy ranging from -1.53 eV to -1.69 eV depending on the bonding arrangement (episulfide or thioether; ‘l’ or ‘d’ orientation). This value is greater than half of a C-S covalent bond energy of ~ 2.7 eV,^{30,31} suggesting strong chemical bonding between the tube and S. For thioether-type adsorption, with the S arranged between a broken carbon-carbon bond, the binding is stronger along the short axis (‘d’) than along the long axis (‘l’) by 0.16 eV. This finding is consistent with previous studies of oxygen dopants on (6,5) SWCNT,¹⁶ and suggests that the binding of the sulfur on the CNT is in-

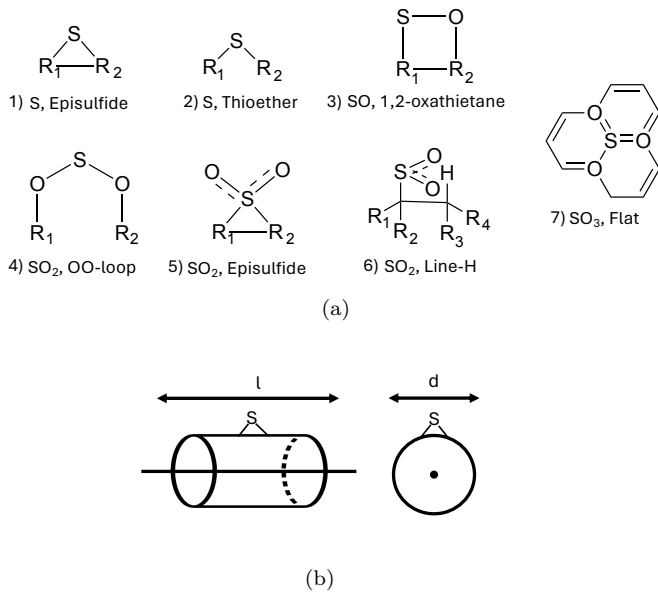


Figure 2. a) The orientation of the different sulfur compounds studied relative to the carbon atoms (R_x) of the SWCNT. b) Illustration of the two different orientations of the sulfur compounds relative to the SWCNT tube axis with a single sulfur atom shown as an example. The cylinder represents the (6,5) SWCNT.

fluenced by its orientation. This anisotropy is not present for the SO molecule, with both the ‘l’ and ‘d’ directions predicted to have a binding energy of -0.56 eV. SO_2 and SO_3 display much weaker binding to the surface, more consistent with physisorption. For SO_2 , all configurations studied were predicted to bind with energies ranging from -0.20 eV (no hydrogen) to -0.33 eV (with hydrogen), indicating that hydrogen only slightly enhances the bond strength. For SO_3 , the binding energy is similarly weak at -0.27 eV. That the larger two defects, SO_2 and SO_3 , are physisorbed on the surface is consistent with previous studies on carbon nanotubes^{32–36}

To better understand the binding of SO_x to (6,5) SWCNT, Figure 3 shows the bonding arrangements of select compounds including bond lengths (for all compounds see SI Table S.1). For the sake of comparison, we note that the S-C covalent bond length is ~ 1.8 Å.³⁷ For the atomic S adsorbate, the bond length is $1.83 - 1.88$ Å, close to the covalent bond length, with bond angle between the S and tube of $63.6^\circ - 66.4^\circ$ (depending on orientation). The S-C bond is slightly stretched for SO adsorption (~ 2.05 Å) with the bond angles indicating a tilt towards one of the two carbons on the tube (S-R-R angle: $\sim 66^\circ$ and $\sim 71^\circ$), which we attribute to steric effects due to the presence of the oxygen atom. All the SO_2 and the SO_3 structures show an adsorption distance of ~ 3.0 Å away from the SWCNT surface, consistent with the weak binding. For SO_2 , the bond angles for the OO-loop-d (S-R-R angle: 82.4° and 72.3°) and Episulfide-d (S-R-R angle: 78.3° and 75.9°) structures indicate the molecule adsorbs slightly off of the C-C bond with S in the hollow site, while the hydrogen passivated structure

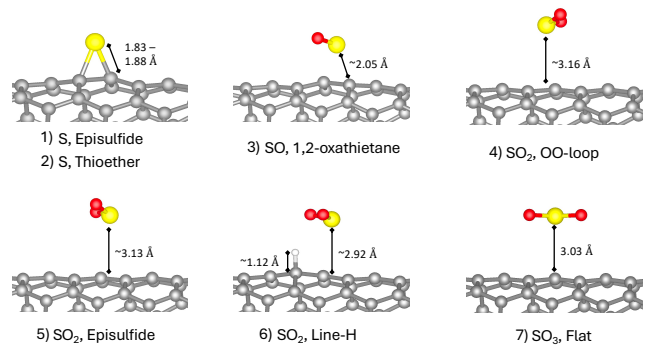


Figure 3. The PBE-D3-predicted adsorption sites of the SO_x structures on (6,5) SWCNT. Relevant bond lengths are labeled.

shows the S in the SO_2 adsorbs on top of a carbon atom (S-R-R angle: 61.2° and 93.8°). SO_3 bond angles (S-R-R angle: 57.5° and 94.0°) also show adsorption of S on top of one of the carbons.

Next, we consider the impact of S, SO, SO_2 , and SO_3 on the electronic structure of (6,5) SWCNT. Based on the predicted bonding for the four sulfur compounds to the tube, we may expect that the S and SO compounds are most likely to occur due to their favorable binding energy and will impact the bandstructure most significantly due to their strong bond with the tube. The band structures of select low-energy configurations for the four compounds are shown in Fig. 4 (see SI Figure S.5 for all band structures).

The near-gap states of the (6,5) SWCNT are of π -type character with a two-fold degeneracy at $\mathbf{k} = 0$ due to the underlying graphitic structure. All the defects presented break the symmetry of the tube, leading to splitting of the nearly-degenerate valence and conduction bands, as has been reported previously for doped (6,5) SWCNT^{5,7–9,16,18,19,25}. This splitting is largest for S and SO (see SI Figure S.4 for more details) as expected from the stronger binding and therefore stronger perturbation to the system. The maximum splitting of the conduction (valence) bands for S, ether-d, S, ether-l, and SO are 0.063 (0.051), 0.20 (0.11) and 0.038 (0.067) eV, respectively. The splitting of the bands for SO_2 is less than 4 meV for both valence and conduction bands, while for SO_3 it is 4 meV for the valence and 0.13 eV for the conduction band.

In addition to symmetry breaking-induced band splitting, both S and SO oriented with the ‘l’ orientation introduce a new unoccupied in-gap state associated with the defect into bandstructure, reducing the gap by up to 0.28 eV for S and 0.08 eV for SO. This in-gap state is associated with a localized defect-centered orbital hybridized with the SWCNT bands as shown in the orbital density plots below the bandstructure. This state is not present for S in the thioether-d configuration for which no defect-centered orbital is present near the gap. SO_2 also introduces an in-gap state; however, this is a flat band with an associated orbital density that is localized on the defect, indicating no interaction with the tube. For

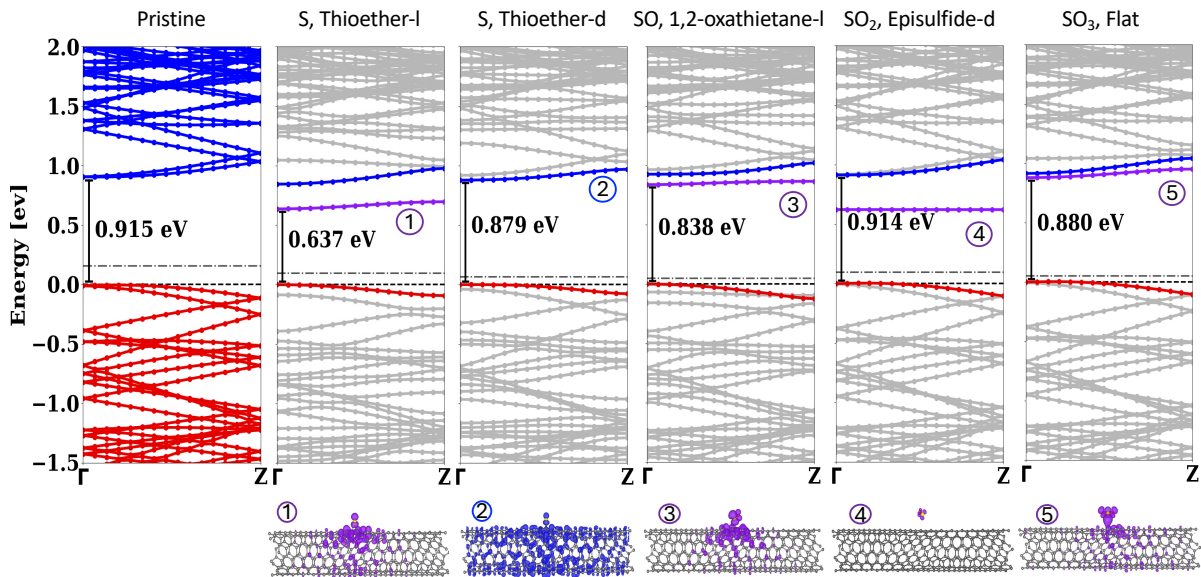


Figure 4. PBE-predicted bandstructure for pristine (6,5) SWCNT and (6,5) SWCNT with the mostly likely adsorbate structures for S, SO, SO₂, and SO₃. Occupied pristine-like valence bands and unoccupied conduction bands are shown in red and blue, respectively, while unoccupied states localized on the defect are in purple. The gray dash-dot line on each band structure represents the Fermi energy. All plots are shifted such that the top of the pristine-like valence band is at zero at $\mathbf{k} = 0$ (indicated by black dash line). The orbital charge density for the lowest energy unoccupied band is shown below the plots with an isosurface that captures 40% of the density.

SO₃, there is an in-gap state resonant with the conduction bands. This state is slightly delocalized over parts of the tube and slightly dispersive. However, we suspect that this mixing between the defect state and conduction may be artificial and due to DFT self-interaction error which results in mixing of two resonant states, as occurs in bond dissociation.³⁸ Thus, we predict that only S and SO can introduce new states into the bandstructure of (6,5) SWCNT, leading to a reduced band gap that varies with the defect.

In summary, we studied four possible SO_x defects (S, SO, SO₂, and SO₃) adsorbed onto (6,5) SWCNT in order to understand their adsorption characteristics and impact on the tube electronic structure. We determined that the two smaller defects, S and SO are strongly bound, with bond lengths consistent with a covalent bond with S, and that there is a strong dependence on the directionality along the tube for the bonds formed by S. Furthermore, based on the binding energies to (6,5) SWCNT, we determine that a mixture of S and SO dopants are responsible for the red-shifted peaks in the PL spectrum of Figure 1. S in the ether-d position is the most strongly bound at 1.6 eV and therefore more likely to form, reducing the gap by ~ 40 meV, slightly smaller than the red-shift of the bright peak in experiment. S in the ether-l is also strongly bound and red-shifts the bandgap by 0.2 eV, consistent with the observed low-energy shoulder in the PL spectrum. SO is also strongly bound to the CNT by 0.56 eV and red-shifts the gap by 80 meV, consistent with the brightest peak in the PL spectrum. Our analysis indicates that both S and SO

have potential for use as a sp³-type defect for use in tuning the photoluminescence energy of the SWCNT.

I. EXPERIMENTAL AND COMPUTATIONAL METHODS

A. Computational details

The electronic structure and adsorption energy of the pristine and doped SWCNT were computed within density functional theory (DFT) as implemented in the Vienna Ab initio Simulation Package (VASP)^{39–43}, with frozen-core projector-augmented wave (PAW) pseudopotentials describing the nuclei and core electrons.^{44,45} The exchange-correlation was treated within the generalized gradient approximation (GGA) of Perdew, Burke, and Ernzerhof (PBE)⁴⁶, with the addition of Grimme D3 van der Waals corrections.⁴⁷ The choice of the PBE functional was made because empirical van der Waals corrections are better suited to PBE, which tends to underbind, rather than LDA which tends to overbind.^{48,49} All SWCNT were placed in a cubic unit cell with 10 Å of vacuum along the two aperiodic directions. Restricted DFT calculations were performed for all but the ‘In-Line-H’ SO₂ system (See Fig. 2(a)), which requires spin-polarized unrestricted DFT. Calculations were performed with a Γ -centered $1 \times 1 \times 2$ k-point mesh with a plane wave energy cutoff of 400 eV. The structure of the full tube and defect were optimized until all forces were less than 0.01 eV/Å. All energies were converged to less than 1×10^{-6} eV. The

optimized lattice vector of the pristine (6,5) SWCNT is $a = 32.4 \text{ \AA}$, $b = 20.0 \text{ \AA}$, and $c = 40.4 \text{ \AA}$ and was kept constant in the periodic direction (c) for all the defective systems.

Surface binding energies were computed for the bound (E_{CNT+SO_x}) and isolated (E_{CNT} , E_{SO_x}) systems as defined in Eq. 1. To obtain the total energy of each system, all three systems were placed in the same cell and all the same computational parameters were applied with the exception of the k-mesh for the SO_x calculation, which was $1 \times 1 \times 1$. For the hydrogen passivated SO_2 structure (structure 6 in Fig. 2(a)), we subtract out the binding energy associated with the hydrogen atom (-1.41 eV), which we determined does not interact with SO_2 . Thus, $E_b^{SO_2} = E_b^{SO_2+H} + 1.41 \text{ eV}$.

B. Experimental Details

Chirality-sorted (6,5) SWCNTs were prepared using a two-step phase separation method, as previously described,^{50,51} and transferred into a 1 wt% sodium dodecyl sulfate (SDS) solution via pressure filtration. The samples were subsequently diluted to an optical density of approximately 0.1 at the E_{11} absorption peak of the (6,5) SWCNTs by 0.5 wt% SDS solutions. Functionalization of the SWCNTs was carried out using a mixture of sodium bicarbonate and sodium dithionite. The functionalized solution was then stored in the dark for further optical characterizations.

Absorption spectra were measured using a Varian Cary 50 UV-Vis spectrophotometer. Photoluminescence spectra were obtained with a Nanolog spectrofluorometer (Horiba Jobin Yvon), which is equipped with a liquid nitrogen-cooled InGaAs detector.

REFERENCES

- ¹P. W. Barone, S. Baik, D. A. Heller, and M. S. Strano, "Near-infrared optical sensors based on single-walled carbon nanotubes," *Nature Materials* **4**, 86–92 (2005).
- ²X. He, H. Htoon, S. K. Doorn, W. H. P. Pernice, F. Pyatkov, R. Krupke, A. Jeantet, Y. Chassagneux, and C. Voisin, "Carbon nanotubes as emerging quantum-light sources," *Nature Materials* **17**, 663–670 (2018).
- ³Q. H. Wang and M. S. Strano, "A bright future for defects," *Nature Chemistry* **5**, 812–813 (2013).
- ⁴X. Ma, N. F. Hartmann, J. K. S. Baldwin, S. K. Doorn, and H. Htoon, "Room-temperature single-photon generation from solitary dopants of carbon nanotubes," *Nature Nanotechnology* **10**, 671–675 (2015).
- ⁵B. M. Weight, A. E. Sifain, B. J. Gifford, D. Kilin, S. Kilina, and S. Tretiak, "Coupling between Emissive Defects on Carbon Nanotubes: Modeling Insights," *The Journal of Physical Chemistry Letters* **12**, 7846–7853 (2021).
- ⁶X. Wang and T. C. Berkelbach, "Excitons in Solids from Periodic Equation-of-Motion Coupled-Cluster Theory," *Journal of Chemical Theory and Computation* **16**, 3095–3103 (2020).
- ⁷S. Ghosh, S. M. Bachilo, R. A. Simonette, K. M. Beckingham, and R. B. Weisman, "Oxygen Doping Modifies Near-Infrared Band Gaps in Fluorescent Single-Walled Carbon Nanotubes," *Science* **330**, 1656–1659 (2010).
- ⁸Y. Piao, B. Meany, L. R. Powell, N. Valley, H. Kwon, G. C. Schatz, and Y. Wang, "Brightening of carbon nanotube photoluminescence through the incorporation of sp³ defects," *Nature Chemistry* **5**, 840–845 (2013).
- ⁹Y. Miyauchi, M. Iwamura, S. Mouri, T. Kawazoe, M. Ohtsu, and K. Matsuda, "Brightening of excitons in carbon nanotubes on dimensionality modification," *Nature Photonics* **7**, 715–719 (2013).
- ¹⁰X. He, N. F. Hartmann, X. Ma, Y. Kim, R. Ihly, J. L. Blackburn, W. Gao, J. Kono, Y. Yomogida, A. Hirano, T. Tanaka, H. Kataura, H. Htoon, and S. K. Doorn, "Tunable room-temperature single-photon emission at telecom wavelengths from sp³ defects in carbon nanotubes," *Nature Photonics* **11**, 577–582 (2017).
- ¹¹X. He, L. Sun, B. J. Gifford, S. Tretiak, A. Piryatinski, X. Li, H. Htoon, and S. K. Doorn, "Intrinsic limits of defect-state photoluminescence dynamics in functionalized carbon nanotubes," *Nanoscale* **11**, 9125–9132 (2019).
- ¹²J. H. Choi, F. T. Nguyen, P. W. Barone, D. A. Heller, A. E. Moll, D. Patel, S. A. Boppart, and M. S. Strano, "Multimodal Biomedical Imaging with Asymmetric Single-Walled Carbon Nanotube/Iron Oxide Nanoparticle Complexes," *Nano Letters* **7**, 861–867 (2007).
- ¹³Z. Liu, S. Tabakman, K. Welsher, and H. Dai, "Carbon nanotubes in biology and medicine: In vitro and in vivo detection, imaging and drug delivery," *Nano Research* **2**, 85–120 (2009).
- ¹⁴A. Högele, C. Galland, M. Winger, and A. Imamoglu, "Photon Antibunching in the Photoluminescence Spectra of a Single Carbon Nanotube," *Physical Review Letters* **100**, 217401 (2008).
- ¹⁵S.-H. Lohmann, K. J. Trerayapiwat, J. Niklas, O. G. Poluektov, S. Sharifzadeh, and X. Ma, "sp³-Functionalization of Single-Walled Carbon Nanotubes Creates Localized Spins," *ACS Nano* **14**, 17675–17682 (2020).
- ¹⁶X. Ma, L. Adamska, H. Yamaguchi, S. E. Yalcin, S. Tretiak, S. K. Doorn, and H. Htoon, "Electronic Structure and Chemical Nature of Oxygen Dopant States in Carbon Nanotubes," *ACS Nano* **8**, 10782–10789 (2014).
- ¹⁷A. Ishii, X. He, N. F. Hartmann, H. Machiya, H. Htoon, S. K. Doorn, and Y. K. Kato, "Enhanced Single-Photon Emission from Carbon-Nanotube Dopant States Coupled to Silicon Microcavities," *Nano Letters* **18**, 3873–3878 (2018).
- ¹⁸S. Kilina, J. Ramirez, and S. Tretiak, "Brightening of the Lowest Exciton in Carbon Nanotubes via Chemical Functionalization," *Nano Letters* **12**, 2306–2312 (2012).
- ¹⁹N. F. Hartmann, S. E. Yalcin, L. Adamska, E. H. Hároz, X. Ma, S. Tretiak, H. Htoon, and S. K. Doorn, "Photoluminescence imaging of solitary dopant sites in covalently doped single-wall carbon nanotubes," *Nanoscale* **7**, 20521–20530 (2015).
- ²⁰B. M. Weight, B. J. Gifford, S. Tretiak, and S. Kilina, "Interplay between Electrostatic Properties of Molecular Adducts and Their Positions at Carbon Nanotubes," *The Journal of Physical Chemistry C* **125**, 4785–4793 (2021).
- ²¹J. Ramirez, M. L. Mayo, S. Kilina, and S. Tretiak, "Electronic structure and optical spectra of semiconducting carbon nanotubes functionalized by diazonium salts," *Chemical Physics Photophysics of carbon nanotubes and nanotube composites*, **413**, 89–101 (2013).
- ²²A. Saha, B. J. Gifford, X. He, G. Ao, M. Zheng, H. Kataura, H. Htoon, S. Kilina, S. Tretiak, and S. K. Doorn, "Narrow-band single-photon emission through selective aryl functionalization of zigzag carbon nanotubes," *Nature Chemistry* **10**, 1089–1095 (2018).
- ²³B. J. Gifford, A. Saha, B. M. Weight, X. He, G. Ao, M. Zheng, H. Htoon, S. Kilina, S. K. Doorn, and S. Tretiak, "Mod($n,m,3$) Dependence of Defect-State Emission Bands in Aryl-Functionalized Carbon Nanotubes," *Nano Letters* **19**, 8503–8509 (2019).
- ²⁴K. J. Trerayapiwat, S. Lohmann, X. Ma, and S. Sharifzadeh,

- “Tuning spin-orbit coupling in (6,5) single-walled carbon nanotube doped with sp³ defects,” *Journal of Applied Physics* **129**, 014309 (2021).
- ²⁵K. J. Trerayapiwat, X. Li, X. Ma, and S. Sharifzadeh, “Broken Symmetry Optical Transitions in (6,5) Single-Walled Carbon Nanotubes Containing sp³ Defects Revealed by First-Principles Theory,” *Nano Letters* **24**, 667–671 (2024).
- ²⁶A. Goldoni, L. Petaccia, L. Gregoratti, B. Kaulich, A. Barinov, S. Lizzit, A. Laurita, L. Sangaletti, and R. Larciprete, “Spectroscopic characterization of contaminants and interaction with gases in single-walled carbon nanotubes,” *Carbon* **42**, 2099–2112 (2004).
- ²⁷E. Humeres and R. d. F. P. M. Moreira, “Kinetics and mechanisms in flow systems: reduction of SO₂ on carbons,” *Journal of Physical Organic Chemistry* **25**, 1012–1026 (2012), eprint: <https://onlinelibrary.wiley.com/doi/pdf/10.1002/poc.3001>.
- ²⁸E. Humeres, N. A. Debacher, R. d. F. P. M. Moreira, J. A. Santaballa, and M. Canle, “Reactive Site Model of the Reduction of SO₂ on Graphite,” *The Journal of Physical Chemistry C* **121**, 14649–14657 (2017).
- ²⁹A. Shokuhi Rad, M. Esfahanian, S. Maleki, and G. Gharati, “Application of carbon nanostructures toward SO₂ and SO₃ adsorption: a comparison between pristine graphene and N-doped graphene by DFT calculations.” *Journal of Sulfur Chemistry* **37**, 176–188 (2016).
- ³⁰“Covalent Bond Energies,” .
- ³¹“Fundamentals of Chemical Bonding,” (2013).
- ³²Y. Chen, S. Yin, Y. Li, W. Cen, J. Li, and H. Yin, “Curvature dependence of single-walled carbon nanotubes for SO₂ adsorption and oxidation,” *Applied Surface Science* **404**, 364–369 (2017).
- ³³S. Yu and W. Yi, “Single-Walled Carbon Nanotubes as a Chemical Sensor for SO₂ Detection,” *IEEE Transactions on Nanotechnology* **6**, 545–548 (2007), conference Name: IEEE Transactions on Nanotechnology.
- ³⁴M. Mittal and A. Kumar, “Carbon nanotube (CNT) gas sensors for emissions from fossil fuel burning,” *Sensors and Actuators B: Chemical* **203**, 349–362 (2014).
- ³⁵F. Yao, D. L. Duong, S. C. Lim, S. B. Yang, H. R. Hwang, W. J. Yu, I. H. Lee, F. Güneş, and Y. H. Lee, “Humidity-assisted selective reactivity between NO₂ and SO₂ gas on carbon nanotubes,” *Journal of Materials Chemistry* **21**, 4502–4508 (2011).
- ³⁶A. Goldoni, R. Larciprete, L. Petaccia, and S. Lizzit, “Single-Wall Carbon Nanotube Interaction with Gases: Sample Contaminants and Environmental Monitoring,” *Journal of the American Chemical Society* **125**, 11329–11333 (2003).
- ³⁷W. Haynes, *CRC Handbook of Chemistry and Physics* (CRC Press, 2016).
- ³⁸A. Ruzsinszky, J. P. Perdew, G. I. Csonka, O. A. Vydrov, and G. E. Scuseria, “Spurious fractional charge on dissociated atoms: Pervasive and resilient self-interaction error of common density functionals,” *The Journal of Chemical Physics* **125**, 194112 (2006).
- ³⁹G. Kresse and J. Furthmüller, “Efficient iterative schemes for ab initio total-energy calculations using a plane-wave basis set,” *Physical Review B* **54**, 11169–11186 (1996).
- ⁴⁰G. Kresse and J. Furthmüller, “Efficiency of ab-initio total energy calculations for metals and semiconductors using a plane-wave basis set,” *Computational Materials Science* **6**, 15–50 (1996).
- ⁴¹G. Kresse and J. Hafner, “Ab initio molecular dynamics for liquid metals,” *Physical Review B* **47**, 558–561 (1993).
- ⁴²G. Kresse and J. Hafner, “Ab initio molecular-dynamics simulation of the liquid-metal–amorphous-semiconductor transition in germanium,” *Physical Review B* **49**, 14251–14269 (1994).
- ⁴³G. Kresse and J. Hafner, “Norm-conserving and ultrasoft pseudopotentials for first-row and transition elements,” *Journal of Physics: Condensed Matter* **6**, 8245–8257 (1994).
- ⁴⁴P. E. Blöchl, “Projector augmented-wave method,” *Physical Review B* **50**, 17953–17979 (1994).
- ⁴⁵G. Kresse and D. Joubert, “From ultrasoft pseudopotentials to the projector augmented-wave method,” *Physical Review B* **59**, 1758–1775 (1999).
- ⁴⁶J. P. Perdew, K. Burke, and M. Ernzerhof, “Generalized Gradient Approximation Made Simple,” *Physical Review Letters* **77**, 3865–3868 (1996).
- ⁴⁷S. Grimme, J. Antony, S. Ehrlich, and H. Krieg, “A consistent and accurate ab initio parametrization of density functional dispersion correction (DFT-D) for the 94 elements H–Pu,” *The Journal of Chemical Physics* **132**, 154104 (2010).
- ⁴⁸L. He, F. Liu, G. Hautier, M. J. T. Oliveira, M. A. L. Marques, F. D. Vila, J. J. Rehr, G.-M. Rignanese, and A. Zhou, “Accuracy of generalized gradient approximation functionals for density-functional perturbation theory calculations,” *Physical Review B* **89**, 064305 (2014).
- ⁴⁹P. Haas, F. Tran, and P. Blaha, “Calculation of the lattice constant of solids with semilocal functionals,” *Physical Review B* **79**, 085104 (2009).
- ⁵⁰J.-S. Chen, K. J. Trerayapiwat, L. Sun, M. D. Krzyaniak, M. R. Wasielewski, T. Rajh, S. Sharifzadeh, and X. Ma, “Long-lived electronic spin qubits in single-walled carbon nanotubes,” *Nature Communications* **14**, 848 (2023).
- ⁵¹J.-S. Chen, A. Dasgupta, D. J. Morrow, R. Emmanuele, T. J. Marks, M. C. Hersam, and X. Ma, “Room Temperature Lasing from Semiconducting Single-Walled Carbon Nanotubes,” *ACS Nano* **16**, 16776–16783 (2022).